ACS APPLIED MATERIALS & INTERFACES

www.acsami.org

Research Article

Evolution of Surface Oxidation on Ta_3N_5 as Probed by a Photoelectrochemical Method

Keyan Li,[#] Botong Miao,[#] Wenjun Fa,[#] Rong Chen, Jing Jin, Kirk H. Bevan,[*] and Dunwei Wang[*]

Cite This: https://doi.org/10.1021/acsami.0c21780

Read Online

ACCESS | Metrics & More | Article Recommendations | Supporting Information

ABSTRACT: In this work, we present an in situ method to probe the evolution of photoelectrochemically driven surface oxidation on photoanodes during active operation in aqueous solutions. A standard solution of $K_4Fe(CN)_6$-KPi was utilized to benchmark the photocurrent and assess progressive surface oxidation on Ta_3N_5 in various oxidizing solutions. In this manner, a proportional increase in the surface oxygen concentration was detected with respect to oxidation time and further correlated with a continuous decline in the photocurrent. To discern how surface oxidation alters the photocurrent, we experimentally and theoretically explored its impact on the surface carrier recombination and the interfacial hole transfer rates. Our results indicate that the sluggish photocurrent demonstrated by oxidized Ta_3N_5 arises because of changes in both rates. In particular, the results suggest that the N−O replacement present on the Ta_3N_5 surface primarily increases the carrier recombination rate near the surface and to a lesser degree reduces the interfacial hole transfer rate. More generally, this methodology is expected to further our understanding of surface oxidation atop other nonoxide semiconductor photoelectrodes and its impact on their operation.

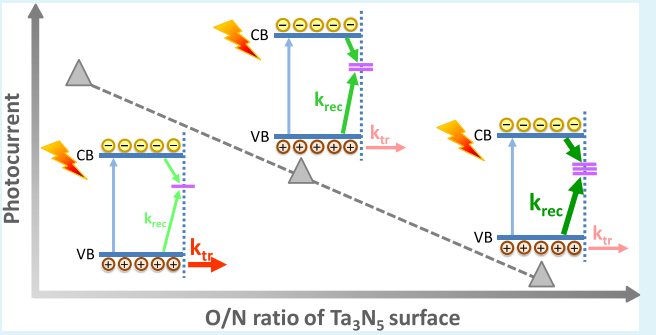

KEYWORDS: *Ta_3N_5, photoelectrochemistry, surface oxidation, water splitting, surface recombination, interfacial carrier transfer*

1. INTRODUCTION

The production of hydrogen and oxygen via photoelectrochemical (PEC) water splitting, as an effective method to capture intermittent solar irradiation and store it in the form of chemical fuels, has attracted wide scientific and technological interest.[1−3] Numerous semiconductors have been explored as photoelectrodes in PEC water splitting cells, with the goal of developing low-cost and stable photoelectrodes with a solar-to-hydrogen (STH) efficiency of over 10%.[4] Over the past 40 years, the research for PEC water splitting has largely focused on metal oxide semiconductor materials,[5] such as Fe_2O_3,[6] WO_3,[7] $SrTiO_3$,[8] $BiVO_4$,[9] and TiO_2.[10] However, the slow charge transport kinetics and/or large band gaps of such metal oxides typically results in low STH efficiencies. However, nonoxide semiconductors (such as silicon, nitrides, and III-V compounds) offer excellent transport properties and smaller band gaps than oxides, but often suffer from instability and photocorrosion during the water splitting processes.[11,12] For example, a p-$GaInP_2$-based photocathode, when paired with a GaAs solar cell in a tandem PEC/photovoltaic arrangement, can split water with an STH efficiency of ∼12%. Unfortunately, this impressive performance cannot be maintained due to the operational formation of a surface oxide film.[13,14] Si-based photoelectrodes also suffer from poor stability, spontaneously oxidizing upon exposure to air/oxygen.[15] Surface oxidation is a common phenomenon in nonoxide materials, which greatly impacts their overall performance. Therefore, methods for quantifying and understanding the manner in which surface oxidation degrades the STH conversion performance of nonoxide based photoelectrodes are urgently needed.

Surface oxidation typically lowers the PEC performance of nonoxides for various reasons, including (1) increased carrier recombination because of the introduction of electron/hole recombination centers; (2) reduced light transmittance because of scattering and absorption of light by the oxide coating; and (3) reduced carrier transfer efficiency from the photoelectrode to the solution.[16] Generally, the emergence of an oxidized surface region facilitates the emergence of recombination centers via the formation of an intermediate amorphous phase. Consequently, surface recombination can compete with interfacial charge transfer, leading to an undesirable reduction in the surface hole concentration able to participate in the water splitting reaction process.[17] Any carriers which recombine, such as holes in a photoanode, cannot participate in the water splitting process. Similarly, an

Received: December 11, 2020
Accepted: March 30, 2021

oxide layer may also lower the efficiency of hole transfer to reaction centers by presenting an additional charge transfer barrier.[18] Taken together, the formation of a surface oxide layer on a nonoxide often lowers the fraction of photogenerated charge carriers that are able to participate in water splitting and adversely impacts the overall reaction kinetics. Various in situ characterization techniques have been developed to observe the surface oxidation of photoelectrodes, such as photoelectrochemical impedance spectroscopy, intensity modulated photocurrent spectroscopy, UV−vis spectroscopy, infrared spectroscopy, Raman spectroscopy, X-ray photoelectron spectroscopy (XPS), and high-resolution transmission electron microscopy.[19−21] Although significant progress has been made, the task of tracking and observing evolving surface oxidation in nonoxide semiconductors under active operation remains an important challenge that needs to be addressed in the field of PEC devices.

Among various nonoxide semiconductors, Ta_3N_5 stands out as a promising PEC material for solar-to-fuel energy conversion owing to its relatively small direct band gap of ∼2.1 eV. Hence, it can absorb visible light up to 600 nm. It also possesses appropriate band edge positions that straddle the water splitting potentials (E_{CB} ∼ −0.3 V_{RHE} and E_{VB} ∼ 1.7 V_{RHE}, here V_{RHE} refers to the voltage relative to the reversible hydrogen electrode potential).[22−24] Thus, theoretically Ta_3N_5 can achieve a maximum photocurrent density of 12.9 mA/cm^2 and a STH efficiency of 15.9% under AM 1.5G solar irradiation.[25,26] However, Ta_3N_5 faces critical stability and photovoltage challenges when utilized for water splitting (including a late turn-on potential V_{on} typically >0.6 V_{RHE}). Both factors originate from surface oxidation via the reaction

$$Ta_3N_5 + 15h^+ + 15OH^- \rightarrow \frac{3}{2}Ta_2O_5 + \frac{5}{2}N_2 + \frac{15}{2}H_2O$$

whereby nitrogen anions are oxidized by photogenerated holes that accumulate at the $Ta_3N_5|H_2O$ interface because of its poor hole transfer kinetics.[27,28] The oxidation process is also likely accompanied by the formation of an amorphous TaO_xN_y phase. The displacement of N by O can increase the surface charge transfer resistance and/or alter interfacial energetics, thereby reducing the driving force for photogenerated charge separation.[18] Both factors lower the photocurrent density. In our previous work, we performed a systematic investigation on how the surface Fermi-level position evolved at the $Ta_3N_5|H_2O$ interface.[29] The thin oxide layer formed on the surface of Ta_3N_5 induced a positive shift in the bulk semiconductor band edges and increased the charge transfer resistance, these factors led to the rapid performance decay of Ta_3N_5 during active operation in a PEC device. However, these prior studies were carried out ex-situ. Hence, the evolution of surface oxidation and its direct impact on performance have not been directly observed under operational conditions. An in situ method that can directly probe the evolution of surface oxidation is expected to shed new light on the process. This work has been developed to meet this critical need.

As has been shown by Domen et al., although Ta_3N_5 electrodes were found to be unstable with respect to water oxidation, they were determined to be fairly stable in aqueous $Fe(CN)_6^{3-}/Fe(CN)_6^{4-}$ solutions under visible light irradiation. This was attributed to the higher activity for $Fe(CN)_6^{4-}$ oxidation compared to water oxidation.[30] Consequently, no noticeable Ta_3N_5 surface oxidation was observed upon PEC operation in aqueous $Fe(CN)_6^{3-}/Fe(CN)_6^{4-}$. Inspired by this observation, in this work we utilize $K_4Fe(CN)_6$ solutions to "freeze" and probe the degree of surface oxidation occurring on Ta_3N_5 arising during PEC water splitting in an oxidizing solution within a given time interval. To this end, we first thoroughly demonstrate that Ta_3N_5 remains stable in an aqueous $K_4Fe(CN)_6$ solution. Subsequently, Ta_3N_5 undergoes active PEC surface oxidation in aqueous solutions with and without various hole scavengers (H_2O_2, Na_2SO_3, and KI) for set durations. Since a lower photocurrent corresponds to increased oxidation at the Ta_3N_5 surface, an aqueous $K_4Fe(CN)_6$ solution can therefore be used to stabilize/halt the surface oxidation process and probe its gradual progression through successive exposure durations to oxidation-prone solutions. Through this process we were able to discern how surface oxidation impacts both surface mediated charge (hole) transfer and interfacial carrier recombination mechanisms. This is accomplished by a detailed comparison between experimental and theoretical analyses at each oxidation exposure interval, producing a direct correlation between the charge transfer efficiency at the solid−electrolyte interface with the gradual evolution of surface oxidation. The photocurrent of oxidized Ta_3N_5 reduces compared to that of a fresh sample, because the interfacial oxidization layer both hinders hole transfer and enhances hole recombination. The central uniqueness of our method lies in its ability to continuously study the same photoelectrode under in situ PEC conditions subjected to different degrees of surface oxidation. The information generated here complements prior studies performed under ex-situ conditions but sheds new light on the underlying physicochemical processes. Importantly, our results were quantitatively corroborated by computational calculations, which provide crucial insight into the physical origins of the observed trends. More broadly, the method demonstrated in this work is expected to be applicable for probing the manner in which surface oxidation impacts the performance of other nonoxide semiconductor photoelectrodes utilized in PEC water splitting.

2. METHODS SECTION

2.1. Preparation of Ta_3N_5 Nanotubes. The Ta_3N_5 sample was synthesized through anodization of a Ta foil to form tantalum oxide nanotubes (NTs) followed by subsequent postannealing in NH_3 to form tantalum nitride according to a previously reported method with slight modifications.[31] For the anodization procedure, a tantalum foil (0.127 mm thick, Alfa Aesar) was first cut into pieces of 1 cm × 3.5 cm in size. Then, one side of the Ta foil was roughened with sandpaper for about 10 min. Afterward, the Ta foil was cleaned by ultrasonication sequentially in acetone, methanol, isopropanol, and deionized (DI) water and dried with compressed air. The electrolyte for anodization was made by mixing 38 mL of sulfuric acid (95−98%, Sigma-Aldrich), 0.4 mL of hydrofluoric acid (48%, Sigma-Aldrich), and 1.6 mL of DI water. The Ta foil was anodized, with another unpolished Ta foil as the counter electrode, at 60 V DC bias for 15 min without stirring. After being thoroughly washed with ethanol and DI water, the as-prepared tantalum oxide NTs were dried in ambient air. The conversion of oxide to nitride was performed in a quartz-tube furnace (Lindberg/Blue M). The temperature was raised from room temperature to 1000 °C at a rate of 10 °C/min and kept at 1000 °C for 2 h. After that, the furnace was naturally cooled down to room temperature. Throughout the process, 75 sccm (standard cubic centimeter per minute) anhydrous NH_3 flowed through the quartz tube, and the pressure in the tube was maintained at 300 Torr.

2.2. Preparation of Photoelectrodes. The Ta_3N_5 sample was scratched on the edge to expose the conductive Ta underneath. A tinned Cu wire was secured to the exposed Ta substrate by Ag epoxy

https://doi.org/10.1021/acsami.0c21780
ACS Appl. Mater. Interfaces XXXX, XXX, XXX−XXX

(M. G. Chemicals). Nonconductive hysol epoxy (Loctite 615) was used to seal the sample, except for the exposed area for testing. Typical electrodes were ~0.05 cm^2 in area. They were etched in a mixture of HF:HNO_3:H_2O (1:2:7 v/v/v) for 1 min before testing in order to remove the oxide on the surface.

2.3. Materials Characterization. XPS was performed on a Surface Science S-Probe ESCA instrument. All binding energies were calibrated with internal standards of the C 1s peak at 284.6 eV.

2.4. (Photo)Electrochemical Measurements. PEC measurements were carried out using a potentiostat (Modulab XM coupled with Modulab XM ECS software) in a three-electrode configuration. The Ta_3N_5 photoanode served as the working electrode (WE), a saturated calomel electrode served as the reference electrode, and a Pt wire served as the counter electrode. The potential was corrected to the RHE scale according to the Nernst equation ($E_{RHE} = E_{SCE} + 0.059$ pH + 0.241). A 505 nm LED light source was utilized with a power density of 25 mW/cm^2. The choice of a monochromic light source proved crucial to corroborating experimental and computational results, where the physical properties of Ta_3N_5 under a single wavelength (e.g., absorption coefficient) are well defined. For the electrolytes, 0.1 M phosphate solution with pH = 10, which is a mixture of 0.1 M K_2HPO_4 and 0.1 M K_3PO_4, was prepared and referred to herein as 0.1 M KPi. The mixture of 0.1 M KPi and 0.1 M $K_4Fe(CN)_6$ (referred herein as $K_4Fe(CN)_6$) was used as a standard solution to test the PEC performance of the samples after being treated in other solutions. Four kinds of surface oxidizing electrolyte solutions were utilized as a basis of comparison: 0.1 M KPi (denoted as KPi), 0.1 M KPi with 0.1 M H_2O_2 (denoted as H_2O_2), 0.1 M KPi with 0.1 M Na_2SO_3 (denoted as Na_2SO_3), and 0.1 M KPi with 0.1 M KI (denoted as KI).

When benchmarking the photocurrent, a freshly prepared Ta_3N_5 photoelectrode was used as the WE and $K_4Fe(CN)_6$ as the electrolyte. The potential was swept from −0.431 to 1.331 V_{RHE} at a rate of 20 mV/s, and the photocurrent of the fresh sample was recorded. After the initial cyclic voltammetry (CV) measurement in $K_4Fe(CN)_6$, the electrode was removed, rinsed with DI water, and purged with nitrogen. Subsequently, it underwent an interval of operation in a surface oxidizing solution. During the 10 s interval of operation in the surface oxidizing solution, the photocurrent was tested at a fixed potential of 1.231 V versus RHE under illumination after which the $J(t)$ data corresponding to this oxidation period were obtained. The electrode was then rinsed and purged according to the same procedure above, and then was dipped in $K_4Fe(CN)_6$ for the in situ CV measurement to obtain the photocurrent. Next, the electrode was cleaned and dipped in the surface oxidizing solution again for photocurrent testing for a longer duration (50 s), such that the total testing time was 1 min from which the sample of 1 min was obtained. Then the photocurrent was again measured in $K_4Fe(CN)_6$. The above procedure was repeated, and samples of 2, 3, 5, 10, and 20 min treatments were obtained after being tested in a given oxidizing solution for total durations of 2, 3, 5, 10, and 20 min, and the photocurrent was measured in $K_4Fe(CN)_6$ accordingly. Electrochemical measurements of Ta_3N_5 photoelectrodes undergoing surface oxidation in KPi, H_2O_2, Na_2SO_3, and KI solutions followed the same procedure.

All other electrochemical measurements were carried out in a $K_4Fe(CN)_6$-KPi solution with pH=10. CV tests of the electrode under light and dark were conducted from 0.331 to 1.631 V and from 0.331 to 2.331 V versus RHE, respectively, at a scan rate of 50 mV/s. For the illuminated and dark open-circuit potential measurements, the V_{oc} values were recorded after a minimum of 15 min of stabilization under open-circuit conditions subject to vigorous stirring. The transient photocurrent response of Ta_3N_5 was recorded every 100 mV from 0.531 to 1.631 V versus RHE at 100 ms per photoelectrode sample.

2.5. Computational and Rate Extraction Methodologies. In the simulation results, the coupled Poisson-continuity equations were numerically solved with appropriate boundary conditions.[32−34] In photocatalytic systems, such as Ta_3N_5, the steady-state electron and hole continuity equations can be expressed in the form

$$\frac{1}{q}\frac{dJ_n}{dx} + G_n - R_n = 0 \tag{1}$$

$$-\frac{1}{q}\frac{dJ_p}{dx} + G_p - R_p = 0 \tag{2}$$

where annihilated and generated electrons/holes are captured through the recombination ($R_{n,p}$) and generation ($G_{n,p}$) rates.[32−36] A detailed discussion on the recombination and generation terms applied can be found in refs.,[32,35] a short summary of the recombination and generation terms can be found in the supporting information. Here, J_n and J_p represent the electron and hole current, respectively, throughout the Ta_3N_5 electrode, and q is the elementary charge. The continuity equations were only solved inside the electrode, as conduction bands are not formed in the liquid where ionic charge transport dominates.[33,34,37] In this regard, appropriate boundary conditions must be applied at both the electrode bulk and liquid interface, respectively. Deep within the Ta_3N_5 electrode, the carrier concentration was set equal to the bulk values (forming Dirichlet boundary conditions for electrons and holes), whereas Neumann boundary conditions were applied at the semiconductor−liquid interface because of the electron ($J_{n|int}$) and hole ($J_{p|int}$) current transfer expressions[33,34]

$$J_{n|int} = -qv_{t,n}(n_s - n_{s0}) \tag{3}$$

$$J_{p|int} = qv_{t,p}(p_s - p_{s0}) \tag{4}$$

Here, n_s and p_s are, respectively, surface electron and hole concentration; n_{s0} and p_{s0} are the corresponding surface electron and hole concentrations in equilibrium; $v_{t,n}$ and $v_{t,p}$ are the electron and hole transfer velocities (essentially rate terms). The interfacial current is given by $J = J_{n|int} + J_{p|int}$.

Poisson's equation was solved self-consistently with the continuity equations because of the coupling between the electrostatic potential and carrier concentrations.[32−34,36] Fundamentally, the potential (ϕ) present in the entire span of the Ta_3N_5-liquid junction arises from interactions between the charges inside Ta_3N_5 (ρ_{sc}) and those in the liquid (ρ_L). It can be expressed in the form

$$\varepsilon\frac{d^2\phi}{dx^2} + \frac{d\phi}{dx}\frac{d\varepsilon}{dx} = -q(\rho_{sc} + \rho_L) \tag{5}$$

where ε represents the spatially varying dielectric constant across the entire system. To solve Poisson's equation, electrostatic boundary conditions must also be appropriately set. Dirichlet boundary conditions were implemented in the bulk of the liquid, whereas a floating potential Neumann boundary condition was applied in the bulk of the semiconductor to capture the photovoltage.[33,34] Further details concerning the computational methodology can be found in the extensive discussions provided in refs.[32,34]

Our photocatalytic simulation assumed solar radiation corresponding to 25 mW/cm^2. The doping concentration of our Ta_3N_5 photoanode was set at approximately 10^{18}/cm^3 and the bandgap was set to 2.2 eV.[38] The 0.1 eV difference between a 2.1 and 2.2 eV band gap has a negligible impact on the inferred simulation results.[38] The recombination rate and transfer rate were estimated from the experimental transient photocurrents based on a model proposed by Peter et al. (see Figures S1 and S2).[39] According to this model, the relationship between the time-dependent current $J(t)$ can be related to the interfacial hole transfer (k_{tr}) and recombination (k_{rec}) rates via the expressions

$$\frac{J(\infty)}{J(0)} = \frac{k_{tr}}{(k_{tr} + k_{rec})} \tag{6}$$

and

$$\frac{J(t) - J(\infty)}{J(0) - J(\infty)} = e^{-t/\tau} \tag{7}$$

https://doi.org/10.1021/acsami.0c21780
ACS Appl. Mater. Interfaces XXXX, XXX, XXX−XXX

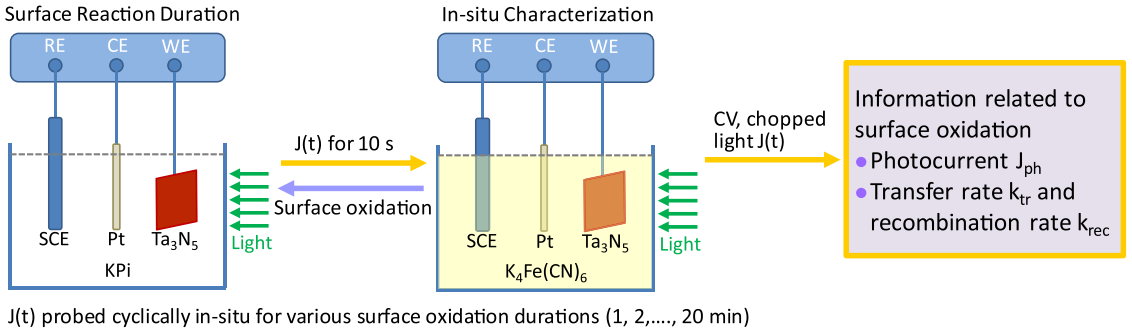

Figure 1. Methodology utilized to probe the surface oxidation of Ta_3N_5 photoanodes after undergoing PEC driven water oxidation for various exposure durations in a KPi containing electrolyte.

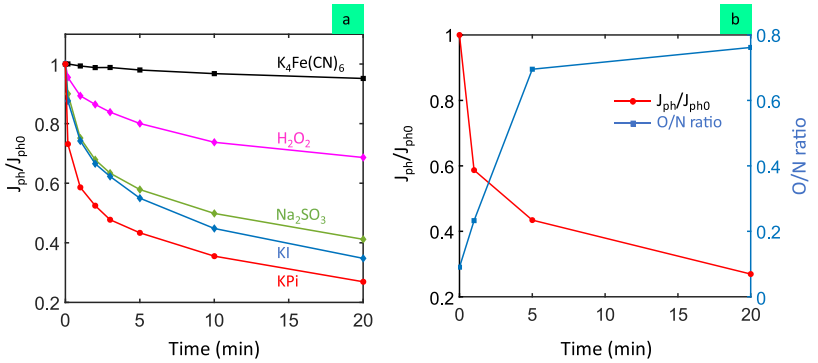

Figure 2. (a) Relative saturation photocurrent densities of Ta_3N_5 as a function of exposure time in KPi with and without hole scavengers; (b) relative saturation photocurrent density and XPS determined O/N ratio for different PEC reaction durations in a pure KPi solution (J_{ph0} is the photocurrent density of fresh Ta_3N_5). All PEC measurements were performed in $K_4Fe(CN)_6$.

Here $J(0)$ is the instantaneous photocurrent (when illumination begins) and $J(\infty)$ is the steady-state photocurrent, with a corresponding interval of exponential decay dictated by eq 7. The lifetime (τ) in eq 7 is related to the recombination and charge transfer rates via $\tau = 1/(k_{tr} + k_{rec})$.By mapping these expressions to chopped illumination transient photocurrent measurements one may experimentally extract the relevant rates and incorporate them in our model to obtain a deeper understanding of the underlying physicochemical processes. Mapping between the electron/hole lifetime and recombination [$\tau_n = \tau_p$ in R_n and R_p] and experimentally extracted k_{rec} values is discussed in the supporting information. The list of simulation parameter values can be found in Table S1.

3. RESULTS AND DISCUSSION

Our method to probe the Ta_3N_5 surface oxidation process is presented in Figure 1. When a Ta_3N_5 photoelectrode undergoes oxidation in KPi containing electrolytes [with or without hole scavengers (Na_2SO_3, KI and H_2O_2)] for varying durations (i.e., 10 s, 1, 2, 3, 5, 10, and 20 min), the degree of surface oxidation will increase with the exposure time. Conversely, when a Ta_3N_5 photoelectrode is removed from these electrolytes, the surface oxidation process is terminated. Because Ta_3N_5 electrodes are stable in $K_4Fe(CN)_6$ during PEC characterization, the degree of surface oxidation will remain unchanged. As a result, by testing Ta_3N_5 in a $K_4Fe(CN)_6$ solution, we can obtain crucial time-resolved information related to the degree of surface oxidation, including: photocurrents via CV curves, as well as charge transfer and recombination rates through transient photocurrent spectra. In effect, we are offered an opportunity to take "measurement snapshots" to record physicochemical information sensitive to the degree of surface oxidation. Similar information is exceedingly difficult to obtain in the original solution where rapid surface evolution would continue unabated.

We begin by demonstrating that Ta_3N_5 can be rendered stable in a $K_4Fe(CN)_6$ solution under operational PEC conditions. As shown in Figure S3(a), when measured in $K_4Fe(CN)_6$, fresh Ta_3N_5 exhibited features of a typical PEC photoanode system, with a saturation photocurrent density of 5.25 mA/cm^2 at 1.23 V versus RHE. After 50 cycles of repeated CV scans, the saturation photocurrent density in $K_4Fe(CN)_6$ decreases slightly to 4.99 mA/cm^2. The stability of Ta_3N_5 in $K_4Fe(CN)_6$ is more clearly demonstrated in Figure 2a, where the saturation photocurrent density was plotted as a function of time. Within the first 20 min of tests, the saturation photocurrent density (J_{ph}) only reduced 4.8% (from 5.22 to 4.97 mA/cm^2). The stability is further demonstrated in Figure S3(b) for even longer time periods. The Ta 4f XPS spectra of fresh Ta_3N_5 and Ta_3N_5 after being tested in $K_4Fe(CN)_6$ for 20 min are provided at the bottom of Figures S4(a) and S4(c). The peaks at 24.7 and 26.6 eV correspond to $Ta4f_{7/2}$ and $Ta4f_{5/2}$ in Ta_3N_5, respectively, whereas the peaks at 25.8 and 27.7 eV are assigned to $Ta4f_{7/2}$ and $Ta4f_{5/2}$ in Ta_2O_5, respectively.[27,40,41] From these XPS results one can conclude that the surface oxygen content does not increase noticeably after extended PEC testing in $K_4Fe(CN)_6$. Thus, Ta_3N_5 remains stable during PEC tests in $K_4Fe(CN)_6$, which can be explained by the lower redox potential of $Fe(CN)_6^{4-}$/$Fe(CN)_6^{3-}$ [compared to that of H_2O/O_2 (1.02 and 1.23 V vs RHE, respectively)] as well as by the absence of oxygen containing intermediates.[29] Therefore, a $K_4Fe(CN)_6$ solution can be used to facilitate in situ characterization of the chemical

https://doi.org/10.1021/acsami.0c21780
ACS Appl. Mater. Interfaces XXXX, XXX, XXX−XXX

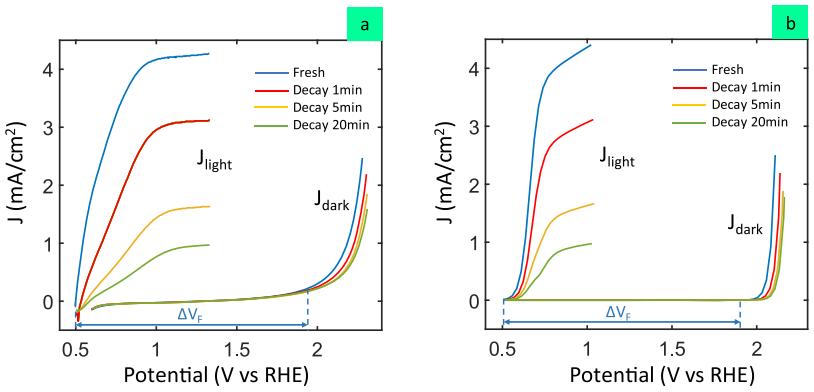

Figure 3. (a) Experimental and (b) computed photocurrent−voltage characteristics and the corresponding dark current−voltage characteristics of the fresh and decayed Ta_3N_5 photoanode exposed to pure KPi for durations corresponding to 1, 5, and 20 min, respectively. PEC-voltage (ΔV_F) of a fresh Ta_3N_5 photoanode is taken as an example here. It is responsible for the shift of the onset potential after illumination. Decayed Ta_3N_5 photoanodes can also be utilized to extract the PEC-voltage.

changes occurring atop Ta_3N_5 photoelectrodes within surface oxidizing solutions.

For the ease of discussion, let us initially examine how surface oxidation evolves in KPi (Figure 2a). After 10 s of exposure to water oxidation conditions, a rapid decay in J_{ph} was observed (from 5.17 mA/cm^2 for fresh sample to 3.78 mA/cm^2 at 10 s, data obtained from Figure S5a). It clearly shows that a fresh Ta_3N_5 electrode undergoes surface oxidation rapidly in the initial PEC reactions, which is consistent with prior reports. At 5 min, J_{ph} drops to 2.24 mA/cm^2 and it further decreases to 1.39 mA/cm^2 at 20 min. The addition of hole scavengers to KPi slows down the photocurrent decay rate, albeit to different degrees. For instance, with KI, J_{ph} drops from 4.51 mA/cm^2 at 10 s to 2.83 mA/cm^2 at 5 min. Likewise, with H_2O_2, J_{ph} decreases from 4.89 mA/cm^2 at 10 s to 4.09 mA/cm^2 at 5 min (again, this is obtained from the CV results in Figure S5). Crucially, the decay in J_{ph} can be directly correlated to an increase in surface oxidation. Figure S4(a) shows the Ta 4f XPS spectra of Ta_3N_5 after being operated in KPi under active PEC operational conditions of varying durations. As the exposure duration in KPi was increased, the peak area corresponding to Ta−O bonding increased as well, whereas the peak area corresponding to Ta−N bonding decreased. This is a clear indication that the lattice N was progressively replaced by O at the surface. The O/N ratio was calculated by taking the ratio of XPS peak areas of the Ta−O bond to that of the Ta−N bond (data may be found in Table S2). Figure 2b plots the change in the relative photocurrent [J_{ph} (red)] against the O/N ratio (blue) as determined by XPS. While this set of data is presented for KPi only, the same was found to hold true for the other solutions investigated (see Figure S4 and Table S2).

With this surface oxidation information in hand, let us now explore how surface oxidation acts in reducing the photocurrent. To this end, the current−voltage characteristics of a Ta_3N_5 photoanode operated in $K_4Fe(CN)_6$ in the dark and under illumination, after being exposed to an aqueous KPi solution for various durations, can be found in Figure 3a. The corresponding theoretical simulations are provided in Figure 3b. Consider first the experimental current−voltage characteristics in Figure 3a. The dark current of the fresh Ta_3N_5 sample was almost undetectable at relatively low biases (<1.5 V vs RHE). Importantly, the dark current exhibited nearly the same magnitudes despite the different degrees of surface oxidation, although some modest decay at higher biases was noticeable with increasing surface oxidation. The results suggest that the impact of surface oxidation on charge transport in the dark is relatively small under low bias (<1.5 V vs RHE). Indeed, in equilibrium, our computational results revealed that the Fermi level (E_F) of Ta_3N_5 is aligned with the electrochemical potential of the $K_4Fe(CN)_6$ solution (see Figure 4a,i to d,i), so that no net current is expected across the interface when the applied bias is small. When a relatively high bias (>1.5 V vs RHE) is applied, an increase of current is expected. Surface oxidation could hinder hole transfer, so that a decrease of current densities at the same high bias would be expected for samples with an increased degree of surface oxidation (see Figure 3a). Interestingly, extending the surface oxidation time from 1 min to 5 min and then 20 min did not appear to further decrease the dark current densities significantly. Importantly, the dark current results indicate that the impact of surface oxidation on charge transfer plateaus after 1 min of exposure in KPi. However, photocurrent properties are impacted upon by both interfacial charge transfer and surface recombination (which is absent in the dark) as we shall explore next.

Next, let us consider the experimental photocurrent−voltage characteristics as shown in Figure 3a. There are two components arising from the nonequilibrium electron and hole populations that contribute to the observed JV curves shown in Figure 3: (1) the photovoltage and (2) the PEC-voltage.[34] In photoanodes, the photovoltage ($V_{ph,OC}$) is the electrostatic shift in the bulk conduction band edges that occurs under open-circuit conditions (as shown in Figure 4). This photovoltage arises due to photogenerated electron−hole pairs separated by the built-in electric field in the open-circuit configuration. Under open-circuit conditions such separated electrons "build up" in the bulk (with nowhere else to go), while separated holes similarly "build up" toward the semiconductor−liquid interface. This proceeds until a steady-counter voltage/field ($V_{ph,OC}$) is reached whereby the recombination rate equals the illumination driven generation rate. When the electron−hole recombination rate increases near the surface, less of a photovoltage ($V_{ph,OC}$) is needed to reach this steady-state open-circuit balance under illumination as shown in Figure 4(a,ii) through 4(d,ii) and Figure 5. Despite its importance, $V_{ph,OC}$ has been less frequently discussed in the literature. By contrast, the PEC-voltage (ΔV_F) is the quasi-Fermi level separation between the bulk

https://doi.org/10.1021/acsami.0c21780
ACS Appl. Mater. Interfaces XXXX, XXX, XXX−XXX

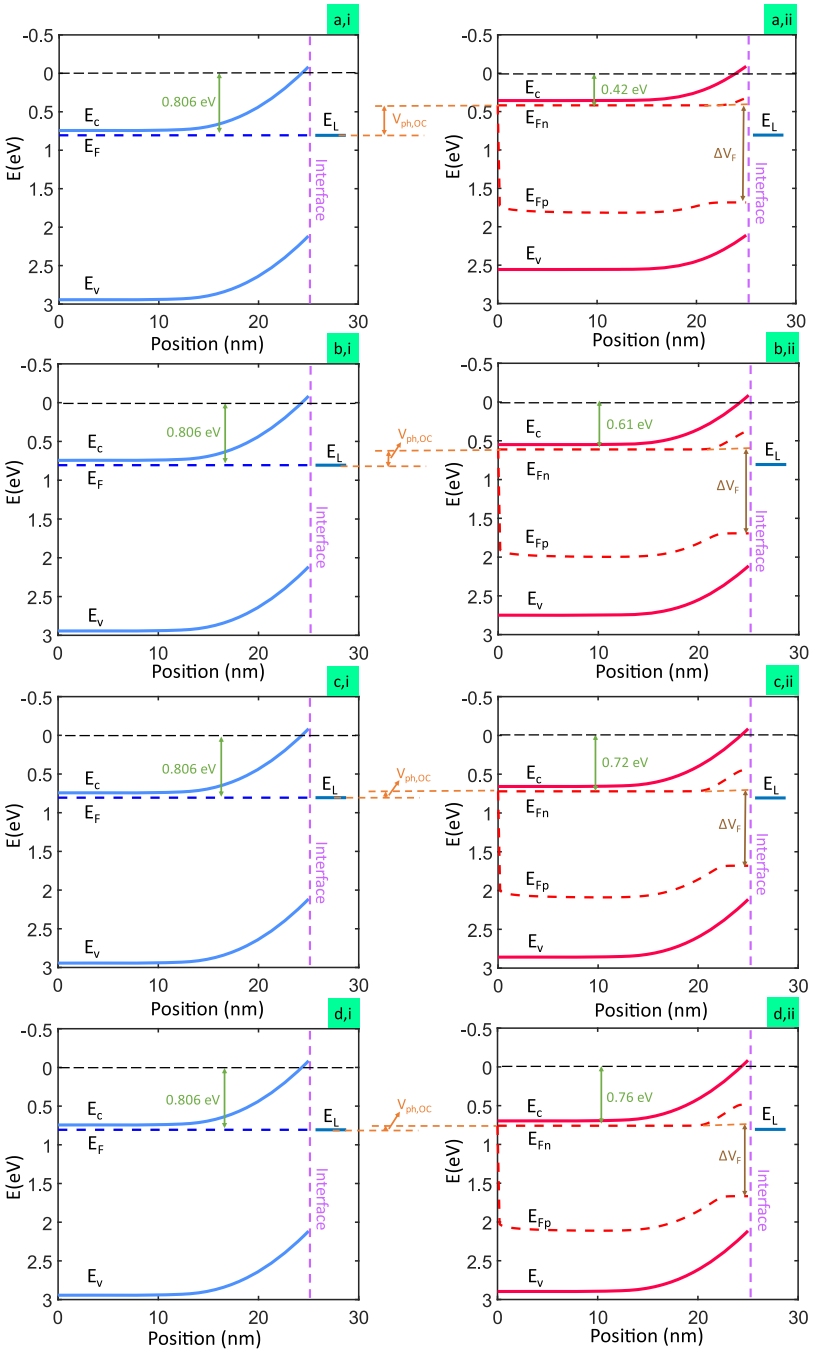

Figure 4. Computed open-circuit energy band diagrams in the dark (a,i–d,i) and under ~25 mW/cm^2 of illumination (a,ii–d,ii) with respect to RHE for fresh and decayed Ta_3N_5 photoanodes exposed to KPi for durations of 1, 5, and 20 min, respectively. Dark open-circuit band diagrams (a,i-d,i) contain the same information, but are replotted to clearly illustrate the change in the illuminated open-circuit photovoltage ($V_{ph,OC}$) as oxidation increases electron–hole recombination and lowers hole transfer near/at the surface.

electron Fermi level and the surface hole quasi-Fermi level (as indicated in Figure 4). The PEC-voltage is reflected as the shift in onset between dark and light current densities at a given overpotential measured with respect to a reference electrode (marked in Figure 3), because illumination provides a nonequilibrium increase in the surface hole concentration for the same offset of the bulk Fermi-level relative to a fixed reference electrode (e.g., RHE). In this regard, it is important to remember that an overpotential plot essentially displays the current relative to an offset between the bulk anode Fermi level and a fixed reference electrochemical potential.[34] Next, we will use the changes of the two values ($V_{ph,OC}$ and ΔV_F) to understand how surface oxidation impacts the performance of Ta_3N_5 as a water oxidation photoanode. A comprehensive discussion on $V_{ph,OC}$ and ΔV_F can be found in ref.[34]

The operational characteristics of this photoanode for various KPi exposure durations are provided by the band diagrams shown in Figure 4. Here, we can see that the RHE open circuit voltage of the fresh anode is around 0.42 V (Figure 4a,ii), and it gradually increases due to the surface oxidation (Figure 4b,ii–d,ii). This is because $V_{ph,OC}$, which counters the built-in band bending, is reduced with increasing

https://doi.org/10.1021/acsami.0c21780
ACS Appl. Mater. Interfaces XXXX, XXX, XXX–XXX

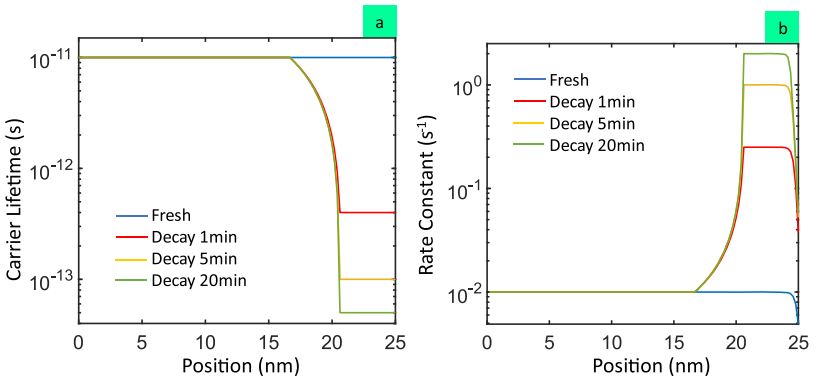

Figure 5. (a) Simulated electron/hole carrier lifetime ($\tau_n = \tau_p$) and (b) recombination rate constant (k_{rec}) of a fresh (blue) and a surface oxidized Ta_3N_5 photoanode simulation in KPi for 1 min (red), 5 min (yellow), and 20 min (green), respectively. Recombination rate constant (k_{rec}) surface values at the solid−liquid interface [at 25 nm in (b)] are fitted to match the experimental values extracted from transient photocurrent measurements as discussed in the context of eqs 6 and 7 and presented in the supporting information.

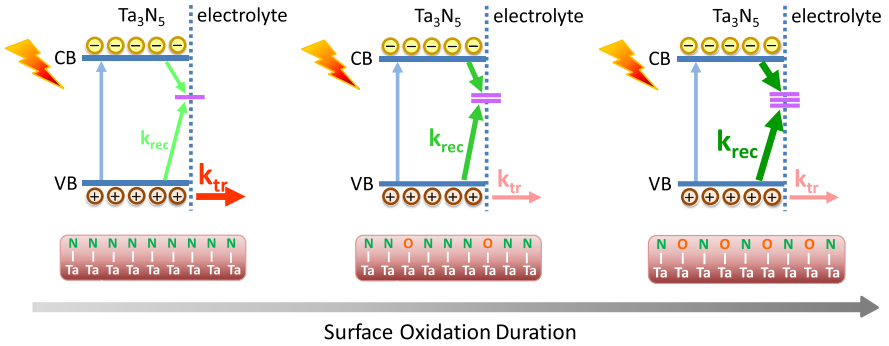

Figure 6. Hypothesized evolution of hole transfer and recombination dynamics with increasing surface oxidation, leading to the reduced photocurrent observed. Hole transfer rate (k_{tr}) decreases in the first stages of oxidation to a small degree, while interfacial hole recombination (k_{rec}) increases substantially with increasing oxidation time.

surface oxidation.[34] Meanwhile, the PEC-voltage is also reduced with increasing oxidation, which can be extracted from the offset between J_{light} and J_{dark} as shown in Figure 3a. The experimental results were closely reproduced by our calculation ones, as shown in Figure 3b. Such a reduction in $V_{ph,OC}$ was previously inferred from our Fermi level measurements,[29] but its origin was not discussed. Here we propose that the reduction of $V_{ph,OC}$, as well the reduction in ΔV_F, is due to the decreased concentration of electrons and holes present on the surface as a result of increased recombination in the oxidized layer. To support this hypothesis, we calculated the carrier lifetimes as shown in Figure 5a based on eqs 6 and 7 through transient photocurrent measurements (see Figure S1). As a benchmark we took the carrier lifetime of fresh Ta_3N_5 to be near constant from the bulk to the surface (blue, Figure 5a), giving rise to a relatively constant recombination rate (k_{rec}) in the bulk. The slight decrease of k_{rec} on the surface arises from the consumption of the surface electrons. Indeed, only a small fraction of electrons recombine with surface holes directly because of the relatively high energy barrier electrons face when approaching the surface. When oxidation is allowed to proceed, the recombination rate increases markedly near the surface of Ta_3N_5 (red, orange, and green in Figure 5). We hypothesize that this is primarily a consequence of the emergence of Shockley−Read−Hall (SRH) recombination centers in an amorphous phase oxidized region.[42,43] Under such conditions, photogenerated holes near the surface rapidly recombine with electrons. Consequently, the photocurrent (J_{ph}) of surface oxidized Ta_3N_5 reduces even more than the dark current (J_{dark}) as shown in Figure 3. This is because the dark current (J_{dark}) is only impacted upon by reductions in k_{tr}, while the photocurrent (J_{ph}) is impacted upon by both k_{tr} and k_{rec}.

Hence, from the dark-current results as shown in Figure 3 we see that the overall hole transfer rate (k_{tr}) because of surface oxidation decreases is measurable but minimal. Increased carrier recombination (via k_{rec}) plays a far more important role in altering the photocurrent densities, and it does so by shifting the semiconductor bulk band edge positions away from the liquid vacuum level, as manifested by a decrease in $V_{ph,OC}$ (see Figure 4). These conclusions are supported by the transient photocurrent spectra in Figures S1 and S2. This understanding is schematically illustrated in Figure 6, where the impact of increasing surface oxidation on Ta_3N_5 is depicted progressively. When Ta_3N_5 is fresh and contains no discernable surface oxidation, holes transfer to the electrolyte and participate in the desired oxidation reaction with ease; this initial process is accompanied by a small fraction of holes undergoing recombination. As surface oxidation increases, surface lattice N anions are replaced by O anions; this oxide growth facilitates the formation of SRH recombination centers that trap holes and electrons. As a result, the recombination rate k_{rec} increases in/near the oxidized region. The greater the degree of oxidation, the more SRH centers are present near the surface; k_{rec} proportionally increases with surface oxidation. To this point, we have gained a fairly clear picture of what happens during continuous surface oxidation to Ta_3N_5. What remains unclear

https://doi.org/10.1021/acsami.0c21780
ACS Appl. Mater. Interfaces XXXX, XXX, XXX−XXX

is the mechanism that leads to the small but measurable reduction in k_{tr}. Peculiarly, the change in k_{tr} appears to be most significant during the first minute of oxidation and its subsequent increase was negligible. We tentatively hypothesize that it is related to a change in the interfacial reaction kinetics related to the difference between the Ta−O and Ta−N bonding. Detailed first-principles calculations and advanced spectroscopy studies would be needed to further validate this hypothesis. From this body of research, however, it is clear that the formation of an oxidation layer leads to electrostatic shift of the bulk band edge position (relative to the liquid vacuum or the reference electrode of choice). This shift is proportional to the degree of surface oxidation and accompanying recombination, which in turn depends on the reaction time. The net result is a decay in the measured photocurrent densities.

4. CONCLUSIONS

By corroborating experimental and computational results, we have demonstrated a methodology for probing the evolution of surface oxidation on nonoxide semiconductor photoelectrodes. In this work, Ta_3N_5 was utilized as a model material. Because of the remarkable stability of Ta_3N_5 photoanodes in aqueous $K_4Fe(CN)_6$, it was used as a benchmark solution to probe PEC characteristics from which the evolution of surface oxidation could be discerned through time-resolved reductions in the photocurrent. It was determined that the surface oxidation of Ta_3N_5 leads to decreased PEC performance through both increased hole recombination and decreased hole transfer. More broadly, this work demonstrates a general experimental and theoretical methodology for exploring the function and physicochemical impact of surface oxidation on the performance of PEC devices.

■ ASSOCIATED CONTENT

Supporting Information

The Supporting Information is available free of charge at https://pubs.acs.org/doi/10.1021/acsami.0c21780.

Transient photocurrent spectra of Ta_3N_5; rate constant versus decay time plots and related data; CV curves of Ta_3N_5 for different cycles; Ta 4f XPS spectra of Ta_3N_5; CV curves of Ta_3N_5; J(t) curves for Ta_3N_5 in various solutions; computed energy band diagrams; theoretical simulation parameter values; full width at half maximum and peak areas of the XPS fits (PDF)

■ AUTHOR INFORMATION

Corresponding Authors

Kirk H. Bevan − *Materials Engineering, McGill University, Montréal, Québec H3A 0C5, Canada;* orcid.org/0000-0001-9884-1403; Email: kirk.bevan@mcgill.ca

Dunwei Wang − *Department of Chemistry, Boston College, Chestnut Hill, Massachusetts 02467, United States;* orcid.org/0000-0001-5581-8799; Email: dunwei.wang@bc.edu

Authors

Keyan Li − *Department of Chemistry, Boston College, Chestnut Hill, Massachusetts 02467, United States;* orcid.org/0000-0003-0467-6684

Botong Miao − *Materials Engineering, McGill University, Montréal, Québec H3A 0C5, Canada*

Wenjun Fa − *Department of Chemistry, Boston College, Chestnut Hill, Massachusetts 02467, United States*

Rong Chen − *Department of Chemistry, Boston College, Chestnut Hill, Massachusetts 02467, United States*

Jing Jin − *Department of Chemistry, Boston College, Chestnut Hill, Massachusetts 02467, United States*

Complete contact information is available at: https://pubs.acs.org/10.1021/acsami.0c21780

Author Contributions

#K.L., B.M., and W.F. contributed equally to this work. K.L., W.F., and R.C. prepared the materials and carried out the PEC measurements. B.M. carried out the calculations in consultation with K.B., K.L., B.M., and W.F. and discussed the results and wrote the manuscript. J.J. carried out the XPS characterizations. D.W. provided guidance in the PEC experiments and result analysis. D.W., K.B., and R.C. modified the manuscript.

Notes

The authors declare no competing financial interest.

■ ACKNOWLEDGMENTS

This work was supported by the National Science Foundation (Grant No. CBET 1703662), the Natural Sciences and Engineering Research Council of Canada, as well as the Fonds de recherche du Québec Nature et technologies.

■ REFERENCES

(1) Yang, W.; Prabhakar, R. R.; Tan, J.; Tilley, S. D.; Moon, J. Strategies for Enhancing the Photocurrent, Photovoltage, and Stability of Photoelectrodes for Photoelectrochemical Water Splitting. *Chem. Soc. Rev.* **2019**, *48*, 4979−5015.

(2) Ye, K.-H.; Li, H.; Huang, D.; Xiao, S.; Qiu, W.; Li, M.; Hu, Y.; Mai, W.; Ji, H.; Yang, S. Enhancing Photoelectrochemical Water Splitting by Combining Work Function Tuning and Heterojunction Engineering. *Nat. Commun.* **2019**, *10*, 1−9.

(3) Landman, A.; Halabi, R.; Dias, P.; Dotan, H.; Mehlmann, A.; Shter, G. E.; Halabi, M.; Naseraldeen, O.; Mendes, A.; Grader, G. S. Decoupled Photoelectrochemical Water Splitting System for Centralized Hydrogen Production. *Joule* **2020**, *4*, 448−471.

(4) Wang, S.; Liu, G.; Wang, L. Crystal Facet Engineering of Photoelectrodes for Photoelectrochemical Water Splitting. *Chem. Rev.* **2019**, *119*, 5192−5247.

(5) Sivula, K. Metal Oxide Photoelectrodes for Solar Fuel Production, Surface Traps, and Catalysis. *J. Phys. Chem. Lett.* **2013**, *4*, 1624−1633.

(6) Carroll, G. M.; Gamelin, D. R. Kinetic Analysis of Photoelectrochemical Water Oxidation by Mesostructured Co-Pi/A-Fe_2O_3 Photoanodes. *J. Mater. Chem. A* **2016**, *4*, 2986−2994.

(7) Pesci, F. M.; Cowan, A. J.; Alexander, B. D.; Durrant, J. R.; Klug, D. R. Charge Carrier Dynamics on Mesoporous WO_3 During Water Splitting. *J. Phys. Chem. Lett.* **2011**, *2*, 1900−1903.

(8) Cen, J.; Wu, Q.; Yan, D.; Tao, J.; Kisslinger, K.; Liu, M.; Orlov, A. Photoelectrochemical Water Splitting with a $SrTiO_3$:Nb/$SrTiO_3$ n^+−n Homojunction Structure. *Phys. Chem. Chem. Phys.* **2017**, *19*, 2760−2767.

(9) Kim, T. W.; Choi, K.-S. Nanoporous $BiVO_4$ Photoanodes with Dual-Layer Oxygen Evolution Catalysts for Solar Water Splitting. *Science* **2014**, *343*, 990−994.

(10) Lin, Y.; Zhou, S.; Liu, X.; Sheehan, S.; Wang, D. TiO_2/$TiSi_2$ Heterostructures for High-Efficiency Photoelectrochemical H_2O Splitting. *J. Am. Chem. Soc.* **2009**, *131*, 2772−2773.

(11) Gu, J.; Aguiar, J. A.; Ferrere, S.; Steirer, K. X.; Yan, Y.; Xiao, C.; Young, J. L.; Al-Jassim, M.; Neale, N. R.; Turner, J. A. A Graded

Catalytic−Protective Layer for an Efficient and Stable Water-Splitting Photocathode. *Nat. Energy* **2017**, *2*, 1−8.
(12) Ben-Naim, M.; Palm, D. W.; Strickler, A. L.; Nielander, A. C.; Sanchez, J.; King, L. A.; Higgins, D. C.; Jaramillo, T. F. A Spin Coating Method to Deposit Iridium-Based Catalysts onto Silicon for Water Oxidation Photoanodes. *ACS Appl. Mater. Interfaces* **2020**, *12*, 5901−5908.
(13) Khaselev, O.; Turner, J. A. Electrochemical Stability of P-$GaInP_2$ in Aqueous Electrolytes toward Photoelectrochemical Water Splitting. *J. Electrochem. Soc.* **1998**, *145*, 3335.
(14) Gu, J.; Yan, Y.; Young, J. L.; Steirer, K. X.; Neale, N. R.; Turner, J. A. Water Reduction by a P-$GaInP_2$ Photoelectrode Stabilized by an Amorphous TiO_2 Coating and a Molecular Cobalt Catalyst. *Nat. Mater.* **2016**, *15*, 456−460.
(15) Oskam, G.; Hoffmann, P. M.; Schmidt, J. C.; Searson, P. C. Energetics and Kinetics of Surface States at n-Type Silicon Surfaces in Aqueous Fluoride Solutions. *J. Phys. Chem.* **1996**, *100*, 1801−1806.
(16) Gimenž, S.; Bisquert, J. *Photoelectrochemical Solar Fuel Production: From Basic Principles to Advanced Devices*; Springer, 2016.
(17) Kelly, J.; Memming, R. The Influence of Surface Recombination and Trapping on the Cathodic Photocurrent at p-Type III-V Electrodes. *J. Electrochem. Soc.* **1982**, *129*, 730.
(18) He, Y.; Chen, R.; Fa, W.; Zhang, B.; Wang, D. Surface Chemistry and Photoelectrochemistry—Case Study on Tantalum Nitride. *J. Chem. Phys.* **2019**, *151*, 130902.
(19) Tao, X.; Shi, W.; Zeng, B.; Zhao, Y.; Ta, N.; Wang, S.; Abdul, A. A.; Li, R.; Li, C. Photoinduced Surface Activation of Semiconductor Photocatalysts under Reaction Conditions: A Commonly Overlooked Phenomenon in Photocatalysis. *ACS Catal.* **2020**, *10*, 5941−5948.
(20) Tang, P.; Arbiol, J. Engineering Surface States of Hematite Based Photoanodes for Boosting Photoelectrochemical Water Splitting. *Nanoscale Horizons* **2019**, *4*, 1256−1276.
(21) Klotz, D.; Ellis, D. S.; Dotan, H.; Rothschild, A. Empirical in Operando Analysis of the Charge Carrier Dynamics in Hematite Photoanodes by PEIS, IMPS and IMVS. *Phys. Chem. Chem. Phys.* **2016**, *18*, 23438−23457.
(22) Wang, Z.; Inoue, Y.; Hisatomi, T.; Ishikawa, R.; Wang, Q.; Takata, T.; Chen, S.; Shibata, N.; Ikuhara, Y.; Domen, K. Overall Water Splitting by Ta_3N_5 Nanorod Single Crystals Grown on the Edges of $KTaO_3$ Particles. *Nat. Catal.* **2018**, *1*, 756−763.
(23) Xiao, Y.; Feng, C.; Fu, J.; Wang, F.; Li, C.; Kunzelmann, V. F.; Jiang, C.-M.; Nakabayashi, M.; Shibata, N.; Sharp, I. D. Band Structure Engineering and Defect Control of Ta_3N_5 for Efficient Photoelectrochemical Water Oxidation. *Nat. Catal.* **2020**, *3*, 932−940.
(24) Pihosh, Y.; Minegishi, T.; Nandal, V.; Higashi, T.; Katayama, M.; Yamada, T.; Sasaki, Y.; Seki, K.; Suzuki, Y.; Nakabayashi, M. Ta_3N_5-Nanorods Enabling Highly Efficient Water Oxidation Via Advantageous Light Harvesting and Charge Collection. *Energy Environ. Sci.* **2020**, *13*, 1519−1530.
(25) Pihosh, Y.; Nandal, V.; Minegishi, T.; Katayama, M.; Yamada, T.; Seki, K.; Sugiyama, M.; Domen, K. Development of a Core−Shell Heterojunction Ta_3N_5-Nanorods/$BaTaO_2N$ Photoanode for Solar Water Splitting. *ACS Energy Lett.* **2020**, *5*, 2492−2497.
(26) Liu, G.; Ye, S.; Yan, P.; Xiong, F.; Fu, P.; Wang, Z.; Chen, Z.; Shi, J.; Li, C. Enabling an Integrated Tantalum Nitride Photoanode to Approach the Theoretical Photocurrent Limit for Solar Water Splitting. *Energy Environ. Sci.* **2016**, *9*, 1327−1334.
(27) Higashi, M.; Domen, K.; Abe, R. Fabrication of Efficient TaON and Ta_3N_5 Photoanodes for Water Splitting under Visible Light Irradiation. *Energy Environ. Sci.* **2011**, *4*, 4138−4147.
(28) Dang, H. X.; Hahn, N. T.; Park, H. S.; Bard, A. J.; Mullins, C. B. Nanostructured Ta_3N_5 Films as Visible-Light Active Photoanodes for Water Oxidation. *J. Phys. Chem. C* **2012**, *116*, 19225−19232.
(29) He, Y.; Thorne, J. E.; Wu, C. H.; Ma, P.; Du, C.; Dong, Q.; Guo, J.; Wang, D. What Limits the Performance of Ta_3N_5 for Solar Water Splitting? *Chem* **2016**, *1*, 640−655.
(30) Ishikawa, A.; Takata, T.; Kondo, J. N.; Hara, M.; Domen, K. Electrochemical Behavior of Thin Ta_3N_5 Semiconductor Film. *J. Phys. Chem. B* **2004**, *108*, 11049−11053.
(31) Wang, L.; Nguyen, N. T.; Zhou, X.; Hwang, I.; Killian, M. S.; Schmuki, P. Enhanced Charge Transport in Tantalum Nitride Nanotube Photoanodes for Solar Water Splitting. *ChemSusChem* **2015**, *8*, 2615−2620.
(32) Iqbal, A.; Bevan, K. H. The Impact of Boundary Conditions on Calculated Photovoltages and Photocurrents at Photocatalytic Interfaces. *MRS Commun* **2018**, *8*, 466−473.
(33) Iqbal, A.; Bevan, K. H. Simultaneously Solving the Photovoltage and Photocurrent at Semiconductor−Liquid Interfaces. *J. Phys. Chem. C* **2018**, *122*, 30−43.
(34) Miao, B.; Iqbal, A.; Bevan, K. H. Utilizing Band Diagrams to Interpret the Photovoltage and Photocurrent in Photoanodes: A Semiclassical Device Modeling Study. *J. Phys. Chem. C* **2019**, *123*, 28593−28603.
(35) Pierret, R. F. *Semiconductor Device Fundamentals*; Pearson Education India, 1996.
(36) Vasileska, D.; Goodnick, S. M. *Computational Electronics. Synthesis Lectures on Computational Electromagnetics*; Morgan & Claypool Publishers, 2006.
(37) Cendula, P.; Tilley, S. D.; Gimenez, S.; Bisquert, J.; Schmid, M.; Grätzel, M.; Schumacher, J. r. O. Calculation of the Energy Band Diagram of a Photoelectrochemical Water Splitting Cell. *J. Phys. Chem. C* **2014**, *118*, 29599−29607.
(38) Hisatomi, T.; Kubota, J.; Domen, K. Recent Advances in Semiconductors for Photocatalytic and Photoelectrochemical Water Splitting. *Chem. Soc. Rev.* **2014**, *43*, 7520−7535.
(39) Peter, L. M. Energetics and Kinetics of Light-Driven Oxygen Evolution at Semiconductor Electrodes: The Example of Hematite. *J. Solid State Electrochem.* **2013**, *17*, 315−326.
(40) Wang, Z.; Qi, Y.; Ding, C.; Fan, D.; Liu, G.; Zhao, Y.; Li, C. Insight into the Charge Transfer in Particulate Ta_3N_5 Photoanode with High Photoelectrochemical Performance. *Chem. Sci.* **2016**, *7*, 4391−4399.
(41) Jones, D. R.; Gomez, V.; Bear, J. C.; Rome, B.; Mazzali, F.; McGettrick, J. D.; Lewis, A. R.; Margadonna, S.; Al-Masry, W. A.; Dunnill, C. W. Active Removal of Waste Dye Pollutants Using $Ta_3N_5/W_{18}O_{49}$ Nanocomposite Fibres. *Sci. Rep.* **2017**, *7*, 1−16.
(42) Chun, W.-J.; Ishikawa, A.; Fujisawa, H.; Takata, T.; Kondo, J. N.; Hara, M.; Kawai, M.; Matsumoto, Y.; Domen, K. Conduction and Valence Band Positions of Ta_2O_5, TaON, and Ta_3N_5 by UPS and Electrochemical Methods. *J. Phys. Chem. B* **2003**, *107*, 1798−1803.
(43) Chen, Z.; Dinh, H. N.; Miller, E. *Photoelectrochemical Water Splitting*; Springer, 2013.

https://doi.org/10.1021/acsami.0c21780
ACS Appl. Mater. Interfaces XXXX, XXX, XXX−XXX